

Dual Processing of Two-Dimensional Exchange Data in Magic Angle Spinning NMR of Solids

Robert Tycko* and Alan E. Berger†

*Laboratory of Chemical Physics, National Institute of Diabetes and Digestive and Kidney Diseases, National Institutes of Health, Building 5, Room 112, Bethesda, Maryland 20892-0520; and †Naval Surface Warfare Center, Code B10, Building 1470, 17320 Dahlgren Road, Dahlgren, Virginia 22448-5100

Received March 31, 1999; revised July 9, 1999

We discuss procedures for processing data in rotor-synchronized two-dimensional magic angle spinning (2D MAS) NMR exchange measurements for both structural and dynamical studies. We show, both mathematically and experimentally, that there are two distinct data processing procedures that lead to 2D MAS exchange spectra with purely absorptive crosspeaks. One procedure is that described previously by Hagemeyer, Schmidt-Rohr, and Spiess (HSS). The other procedure is related, but different, and leads to crosspeak intensities given by the formulae of Herzfeld, Roberts, and Griffin (HRG). In 2D MAS exchange experiments on doubly ¹³C-labeled L-alanylglycylglycine, we demonstrate that the HSS and HRG crosspeak intensities can be extracted separately from the same data set and contain independent information. Processing and analysis of 2D MAS exchange data with both the HSS and the HRG procedures may enhance utilization of the information content of 2D MAS exchange measurements.

Key Words: solid state NMR; molecular structure; molecular dynamics; two-dimensional spectroscopy; magic angle spinning.

INTRODUCTION

Two-dimensional (2D) exchange spectroscopy, combined with magic angle spinning (MAS) at moderate or slow speeds, has been shown to be a useful technique for investigating slow molecular motions (1–6) or molecular conformations (7–10) in solids, including organic molecular solids (1, 4–6), synthetic polymers (2–4), and biopolymers (7–10). Information about molecular motions or conformations is contained in the intensities of crosspeaks in a 2D spectrum that connect spinning sideband lines arising from two different chemical shielding anisotropy (CSA) tensors or tensor orientations in the two spectral dimensions. A simple radiofrequency (RF) pulse sequence for 2D MAS exchange measurements is shown in Fig. 1. In studies of molecular motions (1–6), the CSA tensors in t_1 and t_2 are associated with the same nucleus, and the change in the CSA tensor between t_1 and t_2 is due to molecular, usually orientational, motion. In studies of molecular conformations (7–10), the CSA tensors in t_1 and t_2 are associated with two different nuclei that are weakly dipole-coupled, and the change in the CSA tensor between t_1 and t_2 is due to exchange of spin

polarization between the two nuclei. In studies of molecular motions, the kinetics can be extracted from the dependence of the spinning sideband crosspeaks on the exchange period τ , while the symmetry can be extracted from the crosspeak intensities in the fully exchanged (i.e., long τ) limit. In studies of molecular conformation, the relative orientation of the two CSA tensors, which contains structural information if the CSA tensors have been characterized, can be extracted from the spinning sideband crosspeak intensities in the fully exchanged limit. This structural information is then purely angular in nature.

As shown originally by Veeman and co-workers (1, 2), it is essential that the RF pulses in the 2D exchange sequence be synchronized with the MAS sample rotation if crosspeaks are to arise only when exchange occurs. In an unsynchronized experiment, crosspeaks appear even if the CSA tensors in t_1 and t_2 are identical. As shown originally by Spiess and colleagues (3, 4), two different types of synchronization must be employed in order to obtain 2D MAS exchange spectra with purely absorptive crosspeaks. In one data set, which we shall call data set I, τ is required to be an integer multiple of the sample rotation period τ_R . In the other, which we shall call data set II, $\tau + t_1$ is required to be an integer multiple of τ_R .

In this paper, we show theoretically and experimentally that there are two different procedures for processing data sets I and II, both resulting in purely absorptive spinning sideband crosspeaks, but with different crosspeak intensities. One processing procedure is that of Hagemeyer, Schmidt-Rohr, and Spiess (HSS) (3). The other leads to crosspeak intensities given by the formulae derived by Herzfeld, Roberts, and Griffin (HRG) in the context of 2D dipolar/chemical shift correlation experiments (11). As discussed below, in certain cases it may be advantageous to perform both the HSS and the HRG processing procedures on the same data set in order to extract maximal information from the data.

THEORY

Following earlier treatments of 2D MAS exchange experiments (2, 3, 4, 8), the NMR signals in data set I due to ex-

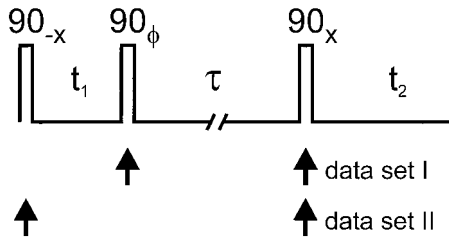


FIG. 1. Simple radiofrequency pulse sequence for 2D MAS exchange measurements. Arrows indicate time points that coincide with the beginning of a rotor period. The two types of rotor synchronization considered in this work are shown. In data set I, the exchange period τ is a multiple of the MAS rotor period. In data set II, $t_1 + \tau$ is a multiple of the rotor period. For the ^{13}C NMR experiments described here, the initial 90_{-x} pulse is replaced by cross-polarization from protons and proton decoupling is applied during the t_1 and t_2 periods.

change from site 1 to site 2 in a molecule with orientation specified by Euler angles α , β , and γ in the MAS rotor can be expressed as

$$S_{\text{Ix}}(\alpha, \beta, \gamma, t_1, t_2) = \text{Re}[f_1(\gamma)f_1(\gamma - \omega_{\text{R}}t_1)^*e^{i\Omega_1t_1}] \\ \times f_2(\gamma + \omega_{\text{R}}t_2)f_2(\gamma)^*e^{i\Omega_2t_2} \quad [1a]$$

$$S_{\text{Iy}}(\alpha, \beta, \gamma, t_1, t_2) = \text{Im}[f_1(\gamma)f_1(\gamma - \omega_{\text{R}}t_1)^*e^{i\Omega_1t_1}] \\ \times f_2(\gamma + \omega_{\text{R}}t_2)f_2(\gamma)^*e^{i\Omega_2t_2} \quad [1b]$$

for $\phi = x$ and $\phi = y$ in Fig. 1. In these expressions, Ω_1 and Ω_2 are the isotropic shifts from the RF carrier frequency in t_1 and t_2 , $\omega_{\text{R}} = 2\pi/\tau_{\text{R}}$, and

$$f_k(\gamma) = \exp\left\{i\frac{\omega_0}{\omega_{\text{R}}}[A_k(\alpha, \beta)\sin 2\gamma - B_k(\alpha, \beta)\cos 2\gamma \\ + C_k(\alpha, \beta)\sin \gamma - D_k(\alpha, \beta)\cos \gamma]\right\}, \quad [2]$$

where $A_k(\alpha, \beta)$, $B_k(\alpha, \beta)$, $C_k(\alpha, \beta)$, and $D_k(\alpha, \beta)$ are real functions of the CSA tensor elements in t_k and ω_0 is the Larmor frequency (4, 8). [Equation [1] differs from equations in previous treatments (8) because the pulse sequence for data set I in Fig. 1 is assumed to begin at time $-t_1$, rather than time 0. $\omega_0 A_k/\omega_{\text{R}}$ in Eq. [2] equals a_k in Eq. [2a] of Ref. (8), etc.] The NMR signals in data set II can be expressed as

$$S_{\text{IIx}}(\alpha, \beta, \gamma, t_1, t_2) = \text{Re}[f_1(\gamma + \omega_{\text{R}}t_1)f_1(\gamma)^*e^{i\Omega_1t_1}] \\ \times f_2(\gamma + \omega_{\text{R}}t_2)f_2(\gamma)^*e^{i\Omega_2t_2} \quad [3a]$$

$$S_{\text{IIy}}(\alpha, \beta, \gamma, t_1, t_2) = \text{Im}[f_1(\gamma + \omega_{\text{R}}t_1)f_1(\gamma)^*e^{i\Omega_1t_1}] \\ \times f_2(\gamma + \omega_{\text{R}}t_2)f_2(\gamma)^*e^{i\Omega_2t_2}. \quad [3b]$$

As in the earlier treatments (3, 4, 8), after pairwise combina-

tion, Fourier series expansion of time-dependent f_k functions, and integration over γ , the signals can be expressed as

$$S_{\text{I}+}(\alpha, \beta, t_1, t_2) \\ = \int_0^{2\pi} d\gamma (S_{\text{Ix}} + iS_{\text{Iy}}) \\ = \sum_{M,N=-\infty}^{+\infty} A_{M,N} \exp[i(M\omega_{\text{R}}t_1 + N\omega_{\text{R}}t_2 + \Omega_1t_1 + \Omega_2t_2)] \quad [4a]$$

$$S_{\text{I}-}(\alpha, \beta, t_1, t_2) \\ = \int_0^{2\pi} d\gamma (S_{\text{Ix}} - iS_{\text{Iy}}) \\ = \sum_{M,N=-\infty}^{+\infty} B_{M,N} \exp[-i(M\omega_{\text{R}}t_1 - N\omega_{\text{R}}t_2 + \Omega_1t_1 - \Omega_2t_2)] \quad [4b]$$

$$S_{\text{II}+}(\alpha, \beta, t_1, t_2) \\ = \int_0^{2\pi} d\gamma (S_{\text{IIx}} + iS_{\text{IIy}}) \\ = \sum_{M,N=-\infty}^{+\infty} B_{M,N} \exp[i(M\omega_{\text{R}}t_1 + N\omega_{\text{R}}t_2 + \Omega_1t_1 + \Omega_2t_2)] \quad [4c]$$

$$S_{\text{II}-}(\alpha, \beta, t_1, t_2) \\ = \int_0^{2\pi} d\gamma (S_{\text{IIx}} - iS_{\text{IIy}}) \\ = \sum_{M,N=-\infty}^{+\infty} A_{M,N} \exp[-i(M\omega_{\text{R}}t_1 - N\omega_{\text{R}}t_2 + \Omega_1t_1 - \Omega_2t_2)] \quad [4d]$$

with

$$A_{M,N} = (F_M^{(1)})^* F_N^{(2)} G_{M-N}^{(1,2)} \quad [5a]$$

$$B_{M,N} = F_M^{(1)} F_N^{(2)} R_{M+N}^{(1,2)} \quad [5b]$$

$$F_N(\alpha, \beta)^{(k)} = \frac{1}{2\pi} \int_0^{2\pi} d\gamma e^{-iN\gamma} f_k(\gamma) \quad [6a]$$

$$G_N(\alpha, \beta)^{(j,k)} = \frac{1}{2\pi} \int_0^{2\pi} d\gamma e^{-iN\gamma} f_j(\gamma) f_k(\gamma)^* \quad [6b]$$

$$R_N(\alpha, \beta)^{(j,k)} = \frac{1}{2\pi} \int_0^{2\pi} d\gamma e^{iN\gamma} f_j(\gamma)^* f_k(\gamma)^*. \quad [6c]$$

Further combination of the data according to the HSS procedure yields

$$\begin{aligned} S_{\text{HSS}+}(\alpha, \beta, t_1, t_2) &= \frac{1}{2} (S_{\text{I}+} + S_{\text{II}-}) \\ &= \sum_{M,N=-\infty}^{+\infty} A_{M,N} \cos(M\omega_{\text{R}t_1} + \Omega_1 t_1) \exp[i(N\omega_{\text{R}t_2} + \Omega_2 t_2)] \end{aligned} \quad [7a]$$

$$\begin{aligned} S_{\text{HSS}-}(\alpha, \beta, t_1, t_2) &= \frac{1}{2i} (S_{\text{I}+} - S_{\text{II}-}) \\ &= \sum_{M,N=-\infty}^{+\infty} A_{M,N} \sin(M\omega_{\text{R}t_1} + \Omega_1 t_1) \exp[i(N\omega_{\text{R}t_2} + \Omega_2 t_2)]. \end{aligned} \quad [7b]$$

Standard processing of $S_{\text{HSS}+}$ and $S_{\text{HSS}-}$ (12) yields a 2D spectrum in which the intensity of the crosspeak connecting the M th spinning sideband in t_1 with the N th spinning sideband in t_2 , when averaged over molecular orientations, is $\mathcal{A}_{M,N} = (4\pi)^{-1} \int_0^\pi d\beta \sin \beta \int_0^{2\pi} d\alpha A_{M,N}(\alpha, \beta)$. We have previously shown that $\mathcal{A}_{M,N}$ is purely real (8), so the crosspeaks are all purely absorptive.

An alternative procedure for combining the data is given by

$$\begin{aligned} S_{\text{HRG}+}(\alpha, \beta, t_1, t_2) &= \frac{1}{2} (S_{\text{II}+} + S_{\text{I}-}) \\ &= \sum_{M,N=-\infty}^{+\infty} B_{M,N} \cos(M\omega_{\text{R}t_1} + \Omega_1 t_1) \exp[i(N\omega_{\text{R}t_2} + \Omega_2 t_2)] \end{aligned} \quad [8a]$$

$$\begin{aligned} S_{\text{HRG}-}(\alpha, \beta, t_1, t_2) &= \frac{1}{2i} (S_{\text{II}+} - S_{\text{I}-}) \\ &= \sum_{M,N=-\infty}^{+\infty} B_{M,N} \sin(M\omega_{\text{R}t_1} + \Omega_1 t_1) \exp[i(N\omega_{\text{R}t_2} + \Omega_2 t_2)]. \end{aligned} \quad [8b]$$

Processing of $S_{\text{HRG}+}$ and $S_{\text{HRG}-}$ yields a 2D spectrum with crosspeak intensities equal to $\mathcal{B}_{M,N} = (4\pi)^{-1} \int_0^\pi d\beta \sin \beta \int_0^{2\pi} d\alpha B_{M,N}(\alpha, \beta)$, which correspond to the expressions of HRG (11). $\mathcal{B}_{M,N}$ is also purely real (8). In fact, if σ_1 and σ_2 are the two CSA tensors in a common axis system, then $\mathcal{B}_{M,N}(\sigma_1, \sigma_2) = \mathcal{A}_{-M,N}(-\sigma_1, \sigma_2)$.

$\mathcal{A}_{M,N}$ and $\mathcal{B}_{M,N}$ both depend on the principal values and orientations of the CSA tensors in t_1 and t_2 , and therefore both contain dynamical or structural information. An important distinction between the two forms is that, when the CSA tensor is identical in t_1 and t_2 [i.e., $f_1(\gamma) = f_2(\gamma)$], $\mathcal{A}_{M,N} = 0$ for $M \neq N$ but $\mathcal{B}_{M,N}$ is generally nonzero. Thus, HSS processing produces crosspeaks only if a true exchange process occurs, whereas HRG processing produces crosspeaks in any event. In the experiments described below, the isotropic shifts Ω_1 and Ω_2 are resolved in the MAS spectra. It is then possible to measure separately the crosspeaks that result from exchange (called *intersite* crosspeaks) and the crosspeaks that are independent of exchange (called *intrasite* crosspeaks). The intersite crosspeaks contain structural or dynamical information. For both types of data processing, the crosspeak intensities can be evaluated numerically for any assumed CSA tensors in t_1 and t_2 , using Eqs. [2], [5], and [6]. Quantitative comparisons between experimental data and simulations can then be used to extract structural or dynamical parameters.

Signal decays during t_1 and t_2 due to spin relaxation or dephasing have been suppressed in the above treatment. Of course, if signal decays were truly absent, the 2D spectra would simply be sums of delta functions and it would only be necessary to acquire data sets I or II, but not both. In real experiments, both data sets are necessary to eliminate dispersive components in the 2D spectra (3, 4, 8, 12).

EXPERIMENTAL AND NUMERICAL METHODS

A 30-mg polycrystalline sample of the tripeptide L-alanyl-glycylglycine (AGG), in which 5% of the AGG molecules were ^{13}C -labeled at the carbonyl positions of Ala-1 and Gly-2, was prepared as previously described (7, 8). 2D MAS exchange measurements (7–10) were carried out at a ^{13}C NMR frequency of 188.6 MHz, using a Bruker Instruments DMX-750 spectrometer and a 4-mm Bruker MAS probe. Measurements were performed at room temperature. The MAS speed was $\omega_{\text{R}}/2\pi = 4.695$ kHz. Proton RF amplitudes were 50 kHz.

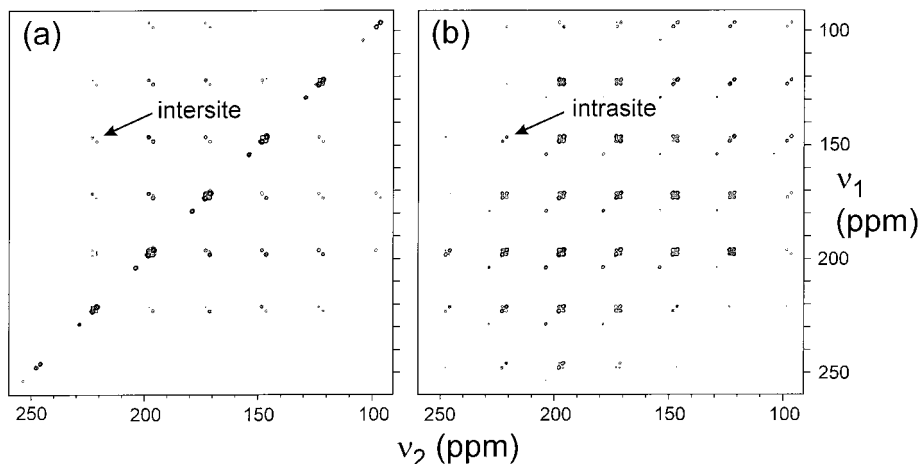


FIG. 2. 2D MAS exchange spectra of doubly ^{13}C -labeled AGG, processed according to the HSS (a) or the HRG (b) procedure. The regions of the 2D spectra that include the labeled carbonyl and natural-abundance carboxyl ^{13}C signals, with spinning sideband orders from -3 to $+3$, are shown. Arrows indicate examples of intersite crosspeaks, which result from exchange between the labeled carbonyl carbons of Ala-1 and Gly-2 and connect spinning sidebands of the two different sites, and intrasite crosspeaks, which are independent of exchange and connect spinning sidebands of a single site. Contour levels increase by factors of 2 and have the same values in (a) and (b). All lineshapes, including those of diagonal peaks, are absorptive in both ν_1 and ν_2 .

^{13}C magnetization was prepared by cross-polarization, using a ramped RF amplitude on the ^{13}C channel. ^{13}C $\pi/2$ pulses were $5\ \mu\text{s}$ in length. The exchange period was $\tau = 512\ \text{ms}$, sufficient for complete exchange between the two ^{13}C -labeled sites. Two hundred fifty-six t_1 points were acquired, with an increment of $25\ \mu\text{s}$ and 16 scans per point per data set. The total signal acquisition time was approximately 14 h. Experimental data were processed with the NMRPipe software package (13).

Crosspeak intensities $\mathcal{A}_{M,N}$ and $\mathcal{B}_{M,N}$ were evaluated numerically as functions of the dihedral angles ϕ and ψ that describe the conformation of AGG at Gly-2, i.e., that determine the relative orientations of the CSA tensors of the two labeled sites. Crosspeak intensities were calculated using trapezoidal quadrature with 32 equal size subintervals for the 2π -periodic integrals over α and γ and composite two-point Gaussian (Gauss–Legendre) quadrature with 32 equal size subintervals for the β integrals over the interval $[0, \pi]$. These calculations assume the chemical bond angles and CSA principal axis system described previously (7, 8). Calculations for Fig. 3 were carried out over a grid of ϕ , ψ values, in increments of 6° . The calculations assume complete exchange at all molecular orientations. The effect of ^{14}N – ^{13}C dipole–dipole coupling on the spinning sideband crosspeak intensities (7, 8) was not included in these calculations. This effect is negligible at the magnetic field strength of the current experiments, as discussed further below. Minima in χ^2 (defined below) were computed using the quasi-Newton (BFGS) option in the program CONMIN, available as TOMS algorithm 500 from NETLIB (<http://www.netlib.org>) (16).

RESULTS AND DISCUSSION

Figure 2 shows the carbonyl region of 2D MAS exchange spectrum of the $^{13}\text{C}_2$ -AGG sample, processed with both the

HSS (Fig. 2a) and the HRG (Fig. 2b) procedures. The principal values of the carbonyl ^{13}C chemical shift tensors of Ala-1 and Gly-2 have previously been determined (7, 8) to be δ_{11} , δ_{22} , $\delta_{33} = 245, 186, 88\ \text{ppm}$ and $242, 182, 89\ \text{ppm}$, respectively, leading to isotropic chemical shifts of 173 and 171 ppm. Both 2D spectra, which derive from the same time-domain data, show diagonal peaks for spinning sideband orders from -3 to $+3$ and crosspeaks that connect the spinning sideband lines of the two different labeled sites. Intersite crosspeaks, which connect spinning sideband lines of the two different labeled sites, appear as doublets oriented perpendicular to the diagonals of the 2D spectra. Intrasite crosspeaks, which connect spinning sideband lines of a single site, appear as doublets oriented parallel to the diagonal. As predicted above, the intrasite crosspeaks are prominent in Fig. 2b but are nearly absent in Fig. 2a. The small residual intrasite crosspeaks in Fig. 2a result from spin–lattice relaxation of ^{14}N nuclei directly bonded to the carbonyl carbons, a process that can change the principal values and orientations of the effective carbonyl CSA tensor of a single ^{13}C site (i.e., the sum of the ^{13}C CSA tensor and the ^{13}C – ^{14}N dipole–dipole coupling tensor) during τ without changing the isotropic shift (7, 8). Intrasite crosspeaks that result from ^{14}N spin–lattice relaxation are weaker in the present experiments than in earlier experiments at lower field because the ^{13}C – ^{14}N coupling is weaker relative to the ^{13}C CSA. As expected, the carboxyl carbon of Gly-3, with an isotropic shift of 179 ppm, contributes crosspeaks to Fig. 2b but not to Fig. 2a.

Figure 3 shows fits of calculated intersite crosspeak intensities to experimental intersite crosspeak intensities (i.e., volumes) extracted from the 2D exchange spectra in Fig. 2. These fits are represented as contour plots of the χ^2 deviation between

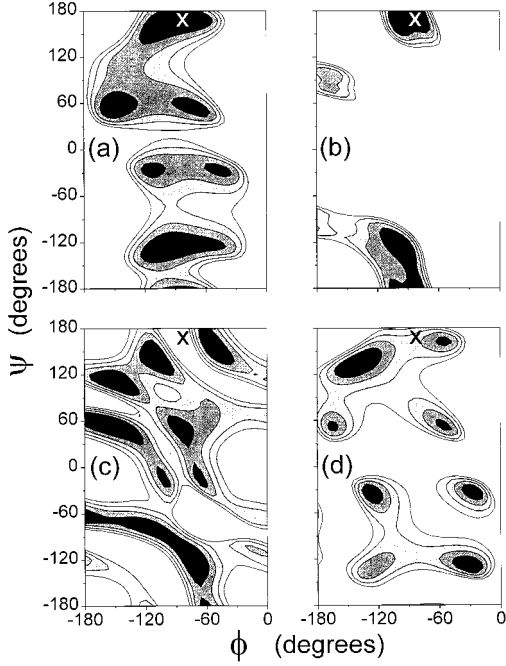


FIG. 3. Fits of calculated spinning sideband crosspeak intensities to experimental crosspeak intensities extracted from the 2D MAS exchange spectra in Fig. 2. Contour plots represent the dependence of the total squared deviation χ^2 between calculated and experimental crosspeaks on the ϕ and ψ dihedral angles assumed in the calculations (see text for details). (a) Calculated HSS crosspeak intensities fit to experimental HSS crosspeak intensities. (b) Calculated HRG crosspeak intensities fit to experimental HRG crosspeak intensities. (c) Calculated HRG crosspeak intensities fit to experimental HSS crosspeak intensities. (d) Calculated HSS crosspeak intensities fit to experimental HRG crosspeak intensities. In all plots, the darkest regions represent $\chi^2 < \chi^2_{\min}$, with $\chi^2_{\min} = 200, 300, 700,$ and 1500 in (a), (b), (c), and (d). White regions represent $\chi^2 > \chi^2_{\max}$, with $\chi^2_{\max} = 1000, 1100, 1500,$ and 2300 in (a), (b), (c), and (d). Contours increase in units of 200. The ϕ, ψ values for Gly-2 in AGG determined from the crystal structure (14) are indicated by crosses.

calculations and experiments as a function of the dihedral angles ϕ and ψ of Gly-2 assumed in the calculations. We define χ^2 by

$$\chi^2(\phi, \psi) = \frac{1}{\sigma^2} \sum_{M,N=-3;M \neq N}^{+3} \{ [E_{M,N}^{(1,2)} - \lambda(\phi, \psi) C_{M,N}^{(1,2)}(\phi, \psi)]^2 + [E_{M,N}^{(2,1)} - \lambda(\phi, \psi) C_{M,N}^{(2,1)}(\phi, \psi)]^2 \} \quad [9a]$$

$$\lambda(\phi, \psi) = \frac{\sum_{M,N=-3;M \neq N}^{+3} [E_{M,N}^{(1,2)} C_{M,N}^{(1,2)}(\phi, \psi) + E_{M,N}^{(2,1)} C_{M,N}^{(2,1)}(\phi, \psi)]}{\sum_{M,N=-3;M \neq N}^{+3} \{ [C_{M,N}^{(1,2)}(\phi, \psi) C_{M,N}^{(1,2)}(\phi, \psi) + C_{M,N}^{(2,1)}(\phi, \psi) C_{M,N}^{(2,1)}(\phi, \psi)] \}} \quad [9b]$$

where σ^2 is the mean squared noise in the experimental spectra, $E_{M,N}^{(i,j)}$ is the experimental crosspeak intensity connecting sideband M of site i with sideband N of site j , and $C_{M,N}^{(i,j)}$ is the calculated intensity (either $\mathcal{A}_{M,N}$ or $\mathcal{B}_{M,N}$) of the same crosspeak for the assumed values of ϕ and ψ . The scaling factor λ minimizes χ^2 at each choice of ϕ and ψ and is the only free fitting parameter besides ϕ and ψ . All other parameters, describing the chemical bonding geometry and CSA tensor orientations relative to the bonding geometry, are fixed as described previously (7, 8). Only negative values of ϕ are plotted in Fig. 3 because the quantities $C_{M,N}^{(i,j)}$ are invariant to the substitution of $-\phi, -\psi$ for ϕ, ψ , implying that $\chi^2(-\phi, -\psi) = \chi^2(\phi, \psi)$ (8).

For Fig. 3, the values $E_{M,N}^{(i,j)}$ with $i \neq j$ are extracted from the 2D exchange spectra by integrating the spectral intensity over rectangular areas that enclose the intersite crosspeaks. The values of σ^2 are determined by integrating the spectral intensity over 160 equal areas centered at positions in the 2D spectra that are well removed from crosspeaks (8). The signal-to-noise ratio, defined as the ratio of the largest $E_{M,N}^{(i,j)}$ with $M \neq N$ and $i \neq j$ to σ , is 24.1 in Fig. 2a and 26.0 in Fig. 2b. The sums in Eqs. [9] are restricted to $M \neq N$ because the intersite crosspeaks with $M = N$ are not sufficiently well resolved from the diagonal peaks to be measured accurately.

According to the AGG crystal structure determined by Subramanian and Lalitha (14), the ϕ and ψ values for Gly-2 are -83° and 170° . The plots in both Figs. 3a and 3b, which show $\chi^2(\phi, \psi)$ for HSS calculations fit to the HSS spectrum and HRG calculations fit to the HRG spectrum, both display regions of minimum $\chi^2(\phi, \psi)$ that are very close to these values. Other local minima in $\chi^2(\phi, \psi)$ are also apparent. These “false” local minima arise because, for any given ϕ, ψ values, there are typically several other ϕ, ψ pairs that correspond to similar, although not identical, relative orientations of the CSA tensors of the two labeled sites (8). Interestingly, several of the local minima in Fig. 3a do not appear in Fig. 3b, i.e., they lead to significantly larger χ^2 values in the HRG spectrum. Thus, a combination of the two forms of data processing allows these local minima to be ruled out with a high level of confidence.

In Fig. 3a, the global minimum in $\chi^2(\phi, \psi)$ is 152.1 at $\phi, \psi = -74.9^\circ, 168.5^\circ$. The next lowest minimum in $\chi^2(\phi, \psi)$ is 162.7 at $\phi, \psi = -99.4^\circ, -126.7^\circ$. In Fig. 3b, the global minimum in $\chi^2(\phi, \psi)$ is 223.2 at $\phi, \psi = -99.3^\circ, 164.3^\circ$. The next lowest minimum in $\chi^2(\phi, \psi)$ is 226.0 at $\phi, \psi = -94.3^\circ, -127.1^\circ$. The larger χ^2 values and the smaller difference between global and next lowest local minimum values for the HRG spectrum in Fig. 3b may be due to the difficulty of accurately determining the experimental intersite crosspeak intensities in the presence of the large and partially overlapping intrasite crosspeaks.

Simultaneous fitting of both 2D spectra (results not shown) does not improve the precision of the ϕ, ψ measurement in this case because the global minima in Figs. 3a and 3b do not coincide precisely. The principal advantage of analyzing both

2D spectra is the elimination of many local minima in χ^2 from consideration as possible ϕ , ψ values.

The differences in calculated crosspeak intensities at various ϕ , ψ combinations depend on the choice of sample spinning frequency ω_R . It is clearly advantageous to perform experiments at a spinning frequency that maximizes the differences between crosspeak intensities at the true ϕ , ψ values and the local minimum ϕ , ψ values. The value $\omega_R/2\pi = 4.695$ kHz used in the experiments in Fig. 2 is close to the value of 5.26 kHz that maximizes the sum \mathcal{S} of the squared differences between the calculated crosspeaks ($C_{M,N}^{(i,j)}$ with $-3 \leq M \neq N \leq 3$; $i, j = 1, 2$ and $2, 1$) at ϕ , $\psi = -83^\circ, 170^\circ$ and at $-96^\circ, -132^\circ$, for a ^{13}C NMR frequency of 188.6 MHz and the carbonyl CSA tensors given above. The latter ϕ , ψ values correspond roughly to the deepest local minima in Figs. 3a and 3b. \mathcal{S} is greater than 90% of its maximum within the interval $3.94 \text{ kHz} \leq \omega_R/2\pi \leq 6.71 \text{ kHz}$.

In cases where the signal-to-noise ratio of the 2D MAS exchange measurements does not permit a reliable differentiation of "true" and false minima in $\chi^2(\phi, \psi)$, additional solid-state NMR measurements, such as measurements of constant-time double-quantum filtered dipolar evolution curves (15), can be carried out on the same doubly ^{13}C -labeled samples.

Figures 3c and 3d show the results of fitting calculated HRG crosspeak intensities to the experimental HSS spectrum and calculated HSS crosspeak intensities to the experimental HRG spectrum, respectively. In both cases, the global minima in $\chi^2(\phi, \psi)$ are substantially greater than in Figs. 3a and 3b. In neither case does the global or any of the local minima correspond to the crystallographic ϕ , ψ values. These results confirm that the HSS and HRG crosspeak intensities for AGG are really quite different from one another. The fact that the position and number of the local minima in Figs. 3a and 3b are different also indicates that the HSS and HRG crosspeak intensities contain independent structural information. It is therefore advantageous to process the 2D MAS exchange data according to both procedures and to carry out fits to both sets of calculated crosspeak intensities, as in Figs. 3a and 3b.

In mathematical terms, the independence of the information content of the HSS and HRG spectra is expressed in the fact that the time-domain NMR signals (i.e., the orientationally averaged functions S_{I_x} , S_{I_y} , S_{I_x} , and S_{I_y}) depend on both the $\mathcal{A}_{M,N}$ and the $\mathcal{B}_{M,N}$ values, as can be seen in Eqs. [4]. Neither the HSS nor the HRG spectrum can be used alone to reconstruct all of the time-domain data. In principle, the two spectra could be used together to reconstruct the time-domain data.

To date, experimental 2D MAS exchange data acquired in both structural (7–10) and dynamical (1–6) studies have been processed exclusively according to the HSS prescription. As discussed above, the HSS prescription leads to crosspeaks only if a true exchange process occurs. This is an important advantage when the exchanging sites do not have resolved sets of spinning sideband lines, i.e., when the isotropic shifts in t_1 and t_2 are the same. However, when the exchanging sites have

resolved lines, it is possible to measure separately the intersite crosspeaks that arise from exchange and the intrasite crosspeaks that are independent of exchange. The HRG and HSS spectra are then both potentially accessible and useful.

In principle, even in the case of unresolved lines, the contribution to the crosspeak intensities from a true exchange process could be separated from the contribution that is independent of exchange in an HRG spectrum, since the intrasite crosspeaks depend only on the carbonyl ^{13}C CSA (and ^{13}C – ^{14}N dipole–dipole coupling in lower fields) and ω_0/ω_R and thus could be calculated separately and subtracted. In practice, factors such as contributions from unresolved natural-abundance signals with uncertain intensities may make such a separation difficult to implement accurately, especially in structural studies of doubly labeled systems of high molecular weight.

Finally, we note that in the 2D MAS experiments of Herzfeld *et al.* (11), unlike in later 2D MAS exchange experiments (1–10), the NMR spectra in the t_1 and t_2 dimensions were spectra of the same nuclear spin determined by two different spin interactions, namely the heteronuclear dipole–dipole coupling in t_1 and the CSA in t_2 . No exchange processes were involved. Thus, the issue of the separation of exchange-dependent from exchange-independent crosspeaks did not arise. Also, the beginnings of both the t_1 and the t_2 periods coincided with the beginnings of rotor periods and the spectra in t_1 were symmetric. It was therefore only necessary to collect one set of signals, namely S_{I_x} .

CONCLUSIONS

We have demonstrated that there are two independent procedures for processing 2D MAS exchange data, both of which yield 2D spectra with purely absorptive crosspeaks. One procedure leads to crosspeak intensities given by the HSS expressions. The other leads to crosspeak intensities given by the HRG expressions. The experimental 2D MAS exchange spectra of AGG illustrate the desirability of carrying out both data processing procedures and fitting calculations of the HSS and HRG crosspeak intensities to the two resulting 2D spectra when the exchanging sites have resolved sets of spinning sideband lines. Use of both the HSS and the HRG crosspeak intensities may increase the information obtained from 2D MAS exchange measurements in both structural and dynamical studies.

ACKNOWLEDGMENTS

A.E.B. gratefully acknowledges support for this work during FY98 from the Applied and Computational Mathematics Program of the Defense Advanced Research Projects Agency. This research was supported in part by a grant from the NIH Intramural AIDS Targeted Antiviral Program.

REFERENCES

1. A. F. de Jong, A. P. M. Kentgens, and W. S. Veeman, Two-dimensional exchange NMR in rotating solids: A technique to study very slow molecular reorientations, *Chem. Phys. Lett.* **109**, 337–342 (1984).
2. A. P. M. Kentgens, E. de Boer, and W. S. Veeman, Ultraslow molecular motions in crystalline polyoxymethylene: A complete elucidation using two-dimensional solid-state NMR, *J. Chem. Phys.* **87**, 6859–6866 (1987).
3. A. Hagemeyer, K. Schmidt-Rohr, and H. W. Spiess, Two-dimensional nuclear magnetic resonance experiments for studying molecular order and dynamics in static and rotating solids, in "Advances in Magnetic Resonance" (W. S. Warren, Ed.), Vol. 13, pp. 85–130, Academic Press, San Diego (1989).
4. Z. Luz, H. W. Spiess, and J. J. Titman, Rotor synchronized MAS two-dimensional exchange NMR in solids: Principles and applications, *Israel J. Chem.* **32**, 145–160 (1992).
5. J. J. Titman, Z. Luz, and H. W. Spiess, Solid-state reactions studied by ^{13}C rotor-synchronized magic angle spinning two-dimensional exchange NMR: 1. Self-diffusion and the tautomeric hydrogen shift in tropolone, *J. Am. Chem. Soc.* **114**, 3756–3765 (1992).
6. J. J. Titman, Z. Luz, and H. W. Spiess, Solid-state reactions studied by ^{13}C rotor-synchronized magic angle spinning two-dimensional exchange NMR: 2. The Cope rearrangement and molecular reorientation in bullvalene, *J. Am. Chem. Soc.* **114**, 3765–3771 (1992).
7. D. P. Weliky and R. Tycko, Determination of peptide conformations by two-dimensional magic angle spinning NMR exchange spectroscopy with rotor synchronization, *J. Am. Chem. Soc.* **118**, 8487–8488 (1996).
8. R. Tycko, D. P. Weliky, and A. E. Berger, Investigation of molecular structure in solids by two-dimensional NMR exchange spectroscopy with magic angle spinning, *J. Chem. Phys.* **105**, 7915–7930 (1996).
9. H. W. Long and R. Tycko, Biopolymer conformational distributions from solid-state NMR: α -Helix and 3_{10} -helix contents of a helical peptide, *J. Am. Chem. Soc.* **120**, 7039–7048 (1998).
10. D. P. Weliky, A. E. Bennett, A. Zvi, J. Anglister, P. J. Steinbach, and R. Tycko, Solid-state NMR evidence for an antibody-dependent conformation of the V3 loop of HIV-1 gp120, *Nature Struct. Biol.* **6**, 141–145 (1999).
11. J. Herzfeld, J. E. Roberts, and R. G. Griffin, Sideband intensities in two-dimensional NMR spectra of rotating solids, *J. Chem. Phys.* **86**, 597–602 (1987).
12. D. J. States, R. A. Haberkorn, and D. J. Ruben, A two-dimensional nuclear Overhauser experiment with pure absorption phase in four quadrants, *J. Magn. Reson.* **48**, 286 (1982).
13. F. Delaglio, S. Grzesiek, G. W. Vuister, G. Zhu, J. Pfeifer, and A. Bax, NMRPipe: A multidimensional spectral processing system based on UNIX pipes, *J. Biomol. NMR* **6**, 277–293 (1995).
14. E. Subramanian and V. Lalitha, Crystal structure of a tripeptide, L-alanylglycylglycine, and its relevance to the poly(glycine)-II type of conformation, *Biopolymers* **22**, 833–838 (1983).
15. A. E. Bennett, D. P. Weliky, and R. Tycko, Quantitative conformational measurements in solid state NMR by constant-time homonuclear dipolar recoupling, *J. Am. Chem. Soc.* **120**, 4897–4898 (1998).
16. D. F. S. Shanno and K. H. Phua, Remark on algorithm 500, *ACM Trans. Math. Software* **6**, 618–622 (1980).